Monthly Notices
of the
ROYAL ASTRONOMICAL SOCIETY

Mon. Not. R. Astron. Soc. **427,** 50–60 (2012) doi:10.1111/j.1365-2966.2012.21686.x

Non-LTE line formation of Fe in late-type stars – II. 1D spectroscopic stellar parameters

K. Lind,[1⋆] M. Bergemann[1] and M. Asplund[1,2]

[1]*Max Planck Institute for Astrophysics, Karl-Schwarzschild Str. 1, 85741 Garching, Germany*
[2]*Research School of Astronomy & Astrophysics, Mount Stromlo Observatory, Cotter Road, Weston Creek, ACT 2611, Australia*

Accepted 2012 July 9. Received 2012 July 8; in original form 2012 February 3

ABSTRACT

We investigate departures from local thermodynamic equilibrium (LTE) in the line formation of neutral and singly ionized iron lines and their impact on spectroscopic stellar parameters. The calculations were performed for an extensive grid of 1D MARCS models of metal-rich and metal-poor late-type dwarfs and giants. We find that iron abundances derived from Fe I lines are increasingly underestimated in hotter, lower surface gravity and more metal-poor stars, in a simple and well-defined pattern, while LTE is usually a realistic approximation for Fe II lines. For the vast majority of dwarfs and giants, the perturbed ionization balance of Fe I and Fe II is the main relevant non-LTE effect to consider in the determination of spectroscopic parameters, while for extremely metal-poor stars and hot giant stars significant impact is seen also on the excitation balance and on the microturbulence determination from Fe I lines.

Key words: atomic data – line: formation – stars: abundances – stars: fundamental parameters – stars: late-type.

1 INTRODUCTION

Measuring the iron content of late-type stars is one of the primary challenges for the field of Galactic archaeology. Due to its large opacity contribution in cool stellar atmospheres, Fe has come to serve as a fundamental reference point for all chemical analysis and its interpretations. Furthermore, the visibility of a wealth of spectral lines with a range of atomic properties and line strengths enables the determination of spectroscopic stellar parameters through the excitation and ionization equilibria. With the knowledge of the star's iron content, effective temperature and surface gravity, we can then acquire further information about the evolution of the star itself, i.e. determine its mass and age, and the evolution of the stellar population it resides in.

However, the low fraction of neutral iron in stellar atmospheres makes its line formation sensitive to departures from local thermodynamic equilibrium (LTE). Traditional LTE analyses of Fe I lines therefore tend to underestimate the true Fe abundance, as is well described in the literature (e.g. Thévenin & Idiart 1999; Gehren, Korn & Shi 2001; Collet, Asplund & Thévenin 2005; Mashonkina et al. 2011).

The success of spectroscopic methods clearly depends on the realism of the atmospheric structure. Even if high precision may be obtained with a very simplistic model, accuracy may or may not. Traditional methods rely on model atmospheres calculated under the assumptions of hydrostatic equilibrium and a 1D geometry. The most critical approximation is the mixing-length description of the convective energy transport. The advent of 3D, radiation-hydrodynamical simulations has shed light on the systematic uncertainties introduced by these simplifying assumptions. In particular, metal-poor stars have been demonstrated to have much cooler line-forming layers than previously thought (see e.g. Asplund 2005 and references therein).

In Paper I of this series (Bergemann et al. 2012), we demonstrated that a modelling technique allowing for departures from LTE can be used to accurately predict iron abundances and spectroscopic stellar parameters for a set of benchmark late-type stars. We specifically illustrated how traditional 1D hydrostatic models successfully meet the ionization and excitation equilibria for solar metallicity stars, but evidently fail to achieve excitation equilibrium at realistic temperatures in metal-poor stars. In particular, low-excitation lines are sensitive to the atmospheric structure, and require a combination of 3D and non-LTE (NLTE) analysis. We further illustrated how the ionization balance of Fe I and Fe II lines can be exploited to infer realistic spectroscopic surface gravities and metallicities also with traditional 1D models, once the effective temperature has been determined by other means. Alternatively, the ionization balance can be used to constrain the effective temperature if the gravity is known by other means.

Due to the increasing numerical complexity, compared with the LTE case, NLTE investigations have previously been limited to individual stars and usually only a handful of spectral lines. For the first time, we present an extensive grid of calculations, with individual NLTE abundance corrections given for thousands of lines in the ultraviolet (UV), optical and near-infrared parts of the

⋆E-mail: klind@mpa-garching.mpg.de

spectrum. The calculations span from ultra-metal-poor to supersolar metallicities and include dwarfs, subgiants and red giant stars. The calculations can easily be extended to an analogous grid of spatially and temporally averaged 3D models (hereafter ⟨3D⟩), once such a grid becomes available from e.g. the STAGGER (Collet, Magic & Asplund 2011) or CO5BOLD collaborations (Ludwig et al. 2009).

2 METHODS

As is customary for late-type stars, we solve the restricted NLTE problem given the assumption of iron as a trace element. Some justification for this methodology is presented in Section 3.3.3. The 1D, NLTE code MULTI, version 2.3 (Carlsson 1986, 1992), was used to simultaneously solve the equations of radiative transfer and statistical equilibrium for a model atom of neutral and singly ionized iron.

2.1 Model atom

The model atom used to establish the statistical equilibrium was presented in detail in Paper I and we give only a summary here. The atom consists of 296 levels of Fe I, 112 levels of Fe II and the Fe III ground state, with experimentally determined and/or theoretically predicted level energies. Levels close in energy were collapsed into superlevels to save computing time. Radiative bound–bound transition probabilities were collected from NIST[1] (Ralchenko, Kramida & Reader 2012) and R. L. Kurucz[2] data bases and photoionization cross-sections were provided by M. Bautista (private communication) (see also Bautista 1997). Rate coefficients for electron impact excitation and ionization were computed using semi-empirical recipes (Seaton 1962; van Regemorter 1962; Allen 1973; Takeda 1994).

The efficiency of excitation and ionization (and charge exchange reactions) induced by collisions with neutral hydrogen is commonly the largest source of uncertainty in statistical equilibrium calculations for late-type stars (see discussion in e.g. Asplund 2005). In the absence of better alternatives, we adopted the Drawin formulae (Steenbock & Holweger 1984) for these processes, and a free scaling parameter ($S_{\rm H}$) that sets the absolute efficiency of the collisions. As explained in Paper I, the scaling factor can be constrained when confronted with observations of stars with surface gravities and effective temperatures accurately known through independent methods. We discuss the impact of our choice of scaling factor, $S_{\rm H} = 1.0$, in Section 3.3.2.

When the atomic level populations had reached convergence, high-resolution NLTE line profiles of 3239 lines of Fe I and 107 lines of Fe II were computed. The lines were selected based on having a non-negligible line strength at solar metallicities and all fall in the wavelength range of 3200–9300 Å. We imposed no further constraints based on the accuracy of atomic data or contribution of blending species in stellar spectra. Hence, lines may or may not be suitable for abundance analysis in a given star. The oscillator strengths were adopted from Kurucz (2007). For 1479 Fe I lines and 95 Fe II lines, ABO theory and the quantum mechanical treatment of pressure broadening by H collisions were implemented for broadening by neutral hydrogen (Barklem, Piskunov & O'Mara 2000; Barklem & Aspelund-Johansson 2005). In the absence of these data, we resort to Unsöld (1955) theory with an enhancement factor of 1.5. Stark broadening is neglected.

[1] http://physics.nist.gov/asd
[2] http://kurucz.harvard.edu/

Table 1. Dimensions of model atmosphere grid.

Parameter	Min.	Max.	Step
$T_{\rm eff}$ (K)	4000	8000	500
$\log g$ [a] (cgs)	1.0	5.0	0.5
[Fe/H]	−5.0	0.5	0.25
$\xi_{\rm t}$ (km s^{-1})	1.0	2.0	1.0

[a] $\log g \geq 2$ for $T_{\rm eff} \geq 6000$ K; $\log g \geq 3$ for $T_{\rm eff} \geq 7000$ K; $\log g \geq 4$ for $T_{\rm eff} = 8000$ K.

2.2 Model atmospheres

We used a grid of 1D, hydrostatic model atmospheres computed with the MARCS code (Gustafsson et al. 2008). The models have standard composition,[3] i.e. scaled solar (Grevesse, Asplund & Sauval 2007) with gradual alpha-enhancement up to 0.4 dex at [Fe/H] ≤ -1.0. The grid dimensions are specified in Table 1. Models that were missing from the original grid were obtained by interpolation or, in some cases, substitution.[4]

2.3 NLTE abundances

Here we base the comparison between LTE and NLTE on equivalent widths (W_λ) rather than synthetic line profiles. Note, however, that differences in lines profiles become important for saturated lines observed at high resolution. For each grid point, we computed the LTE and NLTE equivalent widths for the iron abundance that is identical to the one adopted for the atmosphere. The line strengths increase smoothly with increasing metallicity in a manner similar to a traditional curve of growth. Fig. 1 illustrates the curves derived for a spectral line at a certain effective temperature, surface gravity and microturbulence. The NLTE abundance correction is defined as the difference between the NLTE and LTE curves at a given equivalent width. For practical reasons we introduce a cut towards weak lines at 1 mÅ. Lines weaker than this are not discussed. Our equivalent width integrations are numerically reliable up to ∼1000 mÅ.

Inspection of the NLTE abundance corrections determined for a given set of stellar parameters reveals a strong similarity between lines of similar excitation potential and line strength. In the following discussion we will use the concept of a mean NLTE abundance correction, restricting ourselves to all lines below a certain limit in equivalent width (here 50 mÅ) and above a certain limit in excitation potential (here 2.5 eV) of the lower level. The first restriction is made because abundances of strong lines are through common practice forced into agreement with weaker lines by fine tuning of the microturbulent velocity. The absolute abundances and NLTE corrections derived from microturbulence-sensitive lines are thus of lesser importance. The second restriction to high-excitation lines is motivated by their lower sensitivity to 3D effects compared to low-excitation lines, as discussed in Paper I.

[3] See marcs.astro.uu.se.
[4] When needed and justified, we do not enforce consistency between the microturbulence used to compute the model atmosphere and that used to perform the NLTE calculations, i.e. missing models are replaced with ones of higher/lower microturbulent velocities.

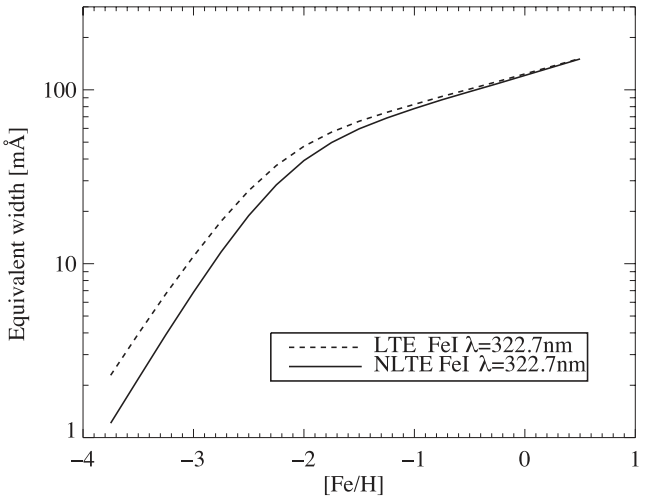

Figure 1. Example LTE and NLTE curves of growth for a UV Fe I transition. The model parameters are $T_{\rm eff} = 6500$ K, $\log g = 4.0$ and $\xi_{\rm t} = 2\,{\rm km\,s^{-1}}$. The NLTE abundance correction at a given equivalent width, $\Delta A({\rm Fe})_{\rm I}$, is defined as the difference between the two curves.

However, in 1D, our atomic model predicts only minor differential NLTE effects for lines of high and low excitation potentials. Fig. 2 illustrates how the mean NLTE abundance correction of unsaturated, high-excitation Fe I lines [$\Delta A({\rm Fe})_{\rm I}$] varies with stellar parameters.

3 DISCUSSION

3.1 Dependence on stellar parameters

As Fig. 2 shows, the departures from LTE have a smooth and simple dependence on stellar parameters. In summary, NLTE abundance corrections increase with decreasing metallicity, increasing effective temperature and decreasing surface gravity. Here we do not aim to disentangle all the contributing factors in order to explain the detailed behaviour quantitatively, but rather we highlight some apparent circumstances that enable a qualitative understanding of the trends.

We focus here on the perturbed ionization balance, established by overionization in Fe I bound–free transitions compared to LTE. We take the term overionization to imply that $n_i P_{ij} - n_j P_{ji} > 0$, where n_i is the level population of a bound state of Fe I and n_j is the ground state of Fe II (notations follow Rutten 2003). $P_{ij} = R_{ij} + C_{ij}$, where R_{ij} is the radiative rate from level i to j and C_{ij} is the corresponding collisional rate. Hence, overionization means that the ionization–recombination balance for a transition is shifted towards more efficient ionization, which tends to depopulate the lower level with respect to LTE. Analogously, overexcitation is adopted for a transition whose excitation–de-excitation balance is shifted towards more efficient excitation. Fig. 3 demonstrates how the total photoionization and photorecombination rates per unit volume ($n_i R_{ij}$ and $n_j R_{ji}$) vary with stellar parameters and the threshold wavelength of the transition. Also shown are the total collisional rates, which in LTE are related by $n_i C_{ij} = n_j C_{ji}$.

The photoionization rate, R_{ij}, is governed by the photoionization cross-sections and the radiation field. In practice, the second dominates the energy dependence of R_{ij}, which exhibits a sharp increase from UV to optical wavelengths and thereafter declines mildly towards infrared wavelengths.[5] The Fe I level population is maximal for the ground state and decreases exponentially with excitation energy. The product $n_i R_{ij}$ thus behaves as shown in Fig. 3, peaking in the UV regime. The recombination rates per unit volume ($n_j R_{ji}$) follow a very similar behaviour but deviate from the photoionization rates as the radiation field deviates from the Planck function.

Collisional rates, C_{ij}, on the other hand, depend on the bound–free collisional cross-sections and the availability of impact electrons and atoms. The impact species have kinetic energy spectra that peak at energies corresponding to infrared wavelengths.[6] In addition, the bound–free collisional cross-sections for electrons and hydrogen atoms increase with decreasing energy gap. These two dependencies outweigh the drop in level population, and the total rate uniformly increases towards longer wavelengths. The relative behaviour of the plotted curves is tightly connected to the sizes of the departures from LTE, through the equations of statistical equilibrium.

Of course, all levels are also coupled by bound–bound radiative rates that can drive the level populations from LTE. Lines, or parts of lines, which are formed close to continuum-forming layers ($\tau_{500} \approx 1$) in the atmosphere react analogously to bound–free transitions to the non-Planckian radiation field. Excitation is thus favoured above de-excitation in the UV and optical in the inner atmosphere, more specifically in layers which are optically thick to the radiation in strong line cores. The accumulated effect of the imbalance in the bound–bound rates is here to enhance the underpopulation of relevant levels of neutral iron. This can be understood because the levels most affected by overexcitation are the lowest excited, while those most affected by overionization are moderately excited (2–4 eV, see Fig. 3). The level populations of Fe I are thus redistributed by line transitions in a way that enhances underpopulation of relevant Fe I levels (<5 eV). We note that in shallow atmospheric layers, where the cores of strong lines become optically thin, different NLTE effects set in that instead favours de-excitation.

We now proceed to interpret the NLTE dependencies on stellar parameters. The overionization is driven by the surplus of UV photons with respect to the Planck function in the atmospheric radiation field. In turn, the size of the $J_\nu - B_\nu$-excess in the UV depends on the steepness of the atmospheric temperature gradient and the efficiency of metal line blocking in this part of the spectrum. We can therefore easily interpret the trend of increasing NLTE effects with decreasing metallicity. It can be seen in Fig. 3 that the gap between the photoionization and photorecombination curves grows larger at lower metallicity, while the relative contribution of radiative and collisional processes is approximately constant (the absolute rates are obviously lowered in accordance with the smaller amount of Fe atoms).

The clear trend of increasing NLTE effects at lower surface gravity can be understood from Fig. 3 as due to the smaller relative strengths of collisional rates, scaling with the number density of iron atoms and the ionizing impact species, with respect to radiative rates, that only scale with the number density of iron.

The temperature gradient steepens sharply at higher effective temperatures, while the flux maximum moves towards shorter wavelengths. In Fig. 3, we see that higher effective temperatures again

[5] Low flux levels in the far-UV in late-type stars suppress the photoionization rates for low-excited levels. Rates for transitions that bridge smaller energy gaps grow increasingly larger as they feel the effect of the stronger radiation field in the optical regime.

[6] At typical temperatures, $kT \sim 0.5$ eV, which corresponds to a kinetic energy peak at 2 μm.

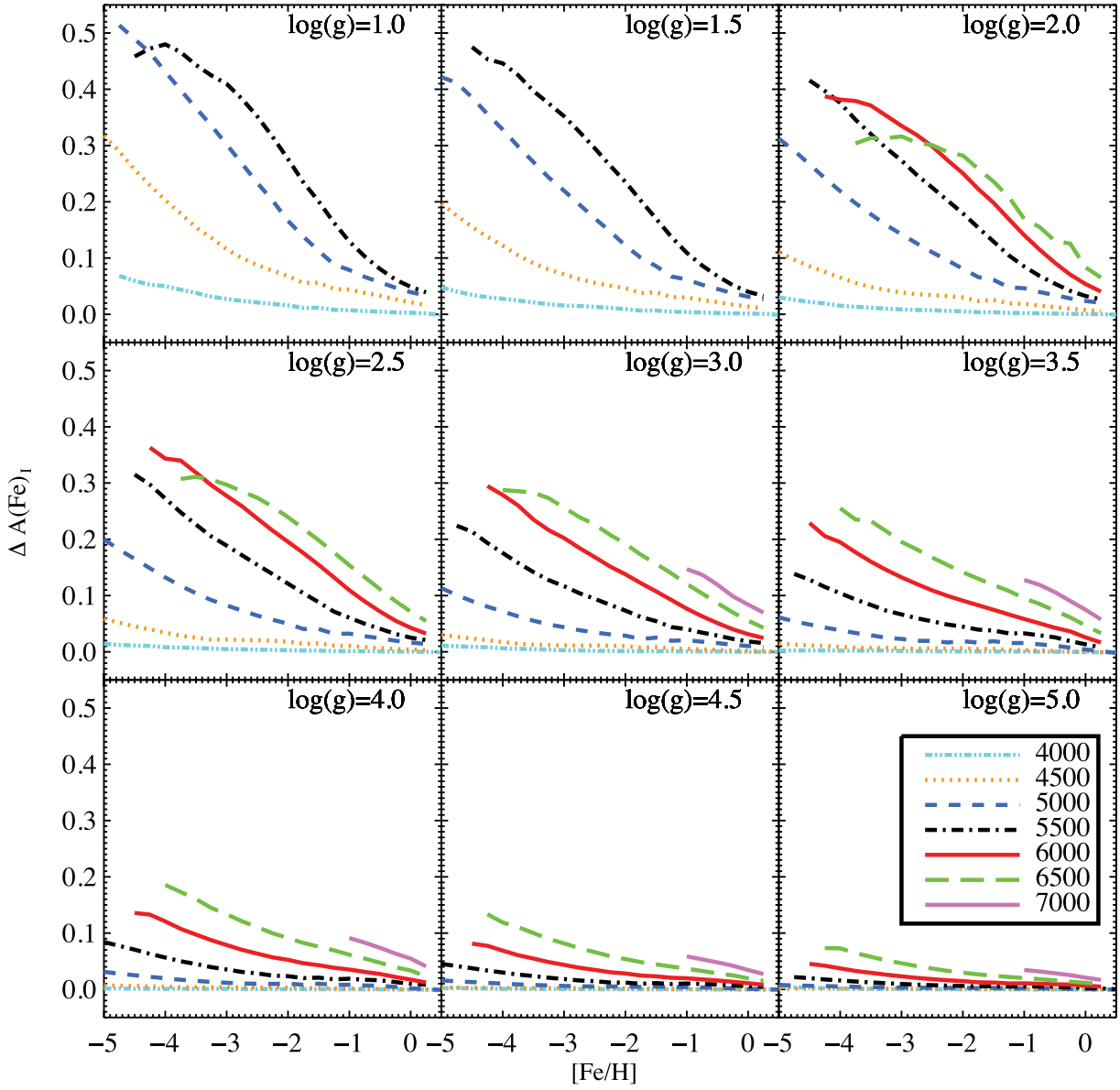

Figure 2. The lines mark the typical sizes of NLTE effects for high-excitation ($E_{\rm exc} > 2.5$ eV), unsaturated ($W_\lambda < 50$ mÅ) Fe I lines and their dependence on stellar parameters. All models shown have $\xi_{\rm t} = 2.0\,{\rm km\,s^{-1}}$.

widen the gap between photoionization and photorecombination curves. In addition, the relative efficiency of collisions with respect to radiative transitions in lessened, since the increased amount of photons outnumbers the increased amount and higher speed of the impact species. All in all, this explains why higher effective temperatures give rise to larger NLTE effects.

Finally, one might ask why only the strengths of Fe I lines are affected by NLTE and not Fe II lines, for which similar arguments as outlined above hold at least qualitatively. Bound–free transitions in Fe II are much less influential on the statistical equilibrium because of the large ionization potential and hence the low number density of Fe III. Furthermore, the three stellar parameter dependencies (lower metallicity, lower surface gravity and higher effective temperature) that give rise to increasing influence from the UV radiation field also act as to raise the relative fraction of singly ionized iron, which usually is the dominant species. A perturbation from the LTE populations clearly has a larger relative influence on a minority species. The well-populated levels from which the visible Fe II transitions originate ($\lesssim$4 eV) are generally close to thermalized throughout the whole atmosphere, while departures from LTE are apparent only above very high excitation energies ($\gtrsim$8 eV).

3.2 Determining stellar parameters

In the following subsection, we will discuss the differences between LTE and NLTE stellar parameters as inferred from Fe I and Fe II lines.

3.2.1 Metallicity

How NLTE affects the metallicity determination can be straightforwardly estimated from Fig. 2. Spectroscopic LTE analyses underestimate the iron abundance derived from Fe I lines by anything between 0.0 and 0.5 dex, the exact value being strongly dependent

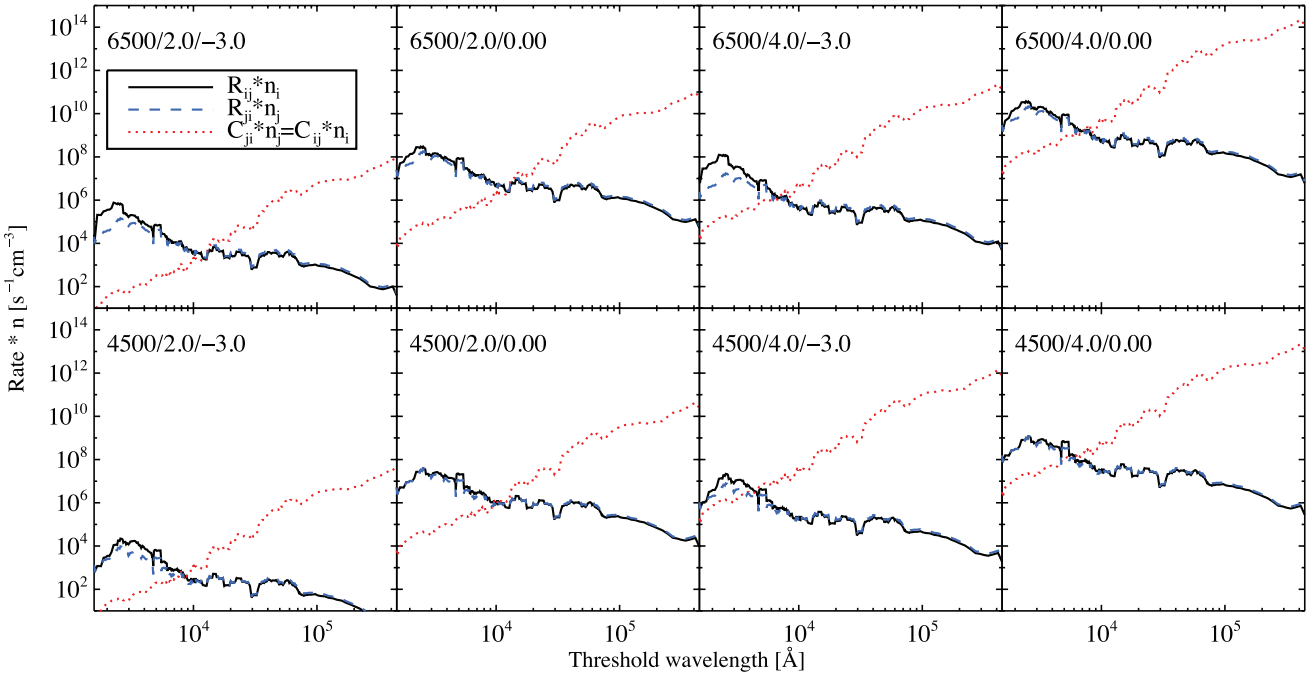

Figure 3. The panels show the total number of Fe I–Fe II ionization and recombination events per unit time and volume for selected models at line-forming layers [$\log(\tau_{500}) = -2$]. The abscissa marks the threshold wavelength, n_i is the LTE level population of the lower level and n_j is the LTE population of the upper level of the corresponding transition, i.e. the ground state of Fe II. The curves have been constructed by applying a smoothing factor of 10 to the individual values, so that each point on the curve represents the average of 10 adjacent rates.

on $T_{\rm eff}$, $\log g$ and [Fe/H]. Abundances derived from Fe II lines are on average not affected at all in models with [Fe/H] > -3. Even at [Fe/H] $= -4$, the corrections for the few lines that are still detectable are smaller than 0.02 dex. We conclude that LTE is a safe assumption for Fe II lines in our parameter space, in line with several previous studies, e.g. Thévenin & Idiart (1999), Korn, Shi & Gehren (2003), Collet et al. (2005), Mashonkina et al. (2011), but also see Cram, Lites & Rutten (1980).

3.2.2 *Surface gravity*

It is common to vary the model surface gravity until agreement is achieved between abundances derived from neutral and singly ionized iron lines, the so-called ionization balance. Since Fe I lines are much less sensitive to surface gravity variations compared to Fe II lines, the metallicity is then practically based on the former. Since Fe I lines are subject to significant NLTE effects, the LTE ionization balance is not always realistic and the surface gravity as well as the metallicity will therefore be underestimated with this method. We have assessed the size of this effect by interpolating LTE curves of growth with varying surface gravity on to the NLTE equivalent widths found at each grid point. Since we are only interested in the difference between LTE and NLTE, the comparison can in principle be inverted and the LTE values chosen as the reference values. This would give very similar results, but since the NLTE equivalent widths are presumably more realistic it is more appropriate to use them as reference. For this comparison we again limit ourselves to unsaturated, high-excitation Fe I and Fe II lines.

The results, i.e. $\Delta\log g = \log g_{\rm NLTE} - \log g_{\rm LTE}$, are shown in Fig. 4. As a rule of thumb, the surface gravity is underestimated by a factor x times the size of the NLTE correction for a given model, in logarithmic units. For dwarfs, $x \approx 2.5$, while for giants the sensitivity increases slightly, $x \approx 3$. Thus, for a metal-poor turn-off star at $T_{\rm eff} = 6500$ K, $\log g = 4.0$, [Fe/H] $= -2$, that has a typical NLTE abundance correction of 0.1 dex, LTE analysis underestimates the surface gravity by 0.25 dex. An important consequence of this behaviour is that metal-poor dwarfs can easily be misclassified as subgiants. Similarly, a red giant star with $T_{\rm eff} = 4500$ K, $\log g = 1.5$, [Fe/H] $= -5$ that has an NLTE abundance correction of 0.2 dex would have its surface gravity underestimated by 0.6 dex in LTE.

3.2.3 *Effective temperature*

Here, we consider two different methods to infer the effective temperature, while the other parameters are kept fixed. First, given a reliable measurement of surface gravity,[7] one may constrain effective temperature through ionization balance. In this case, Fe I-based abundance is effectively brought into agreement with the less temperature-sensitive Fe II lines. The metallicity determination itself thus does not suffer heavy bias in the LTE case, but the optimized effective temperature will be overestimated, by the amount shown in Fig. 5. The calculations were based on weak, high-excitation lines, as before.

Secondly, the effective temperature can be inferred from the excitation balance of Fe I lines, flattening abundance trends with the excitation potential of the lower level of the transition (Fe II lines typically do not span a sufficient range in excitation potential in

[7] This can be provided by an accurate parallax measurement or from stellar evolution calculations. Both methods require a reasonable estimate on effective temperature, in which case the stellar parameter determination may need iteration.

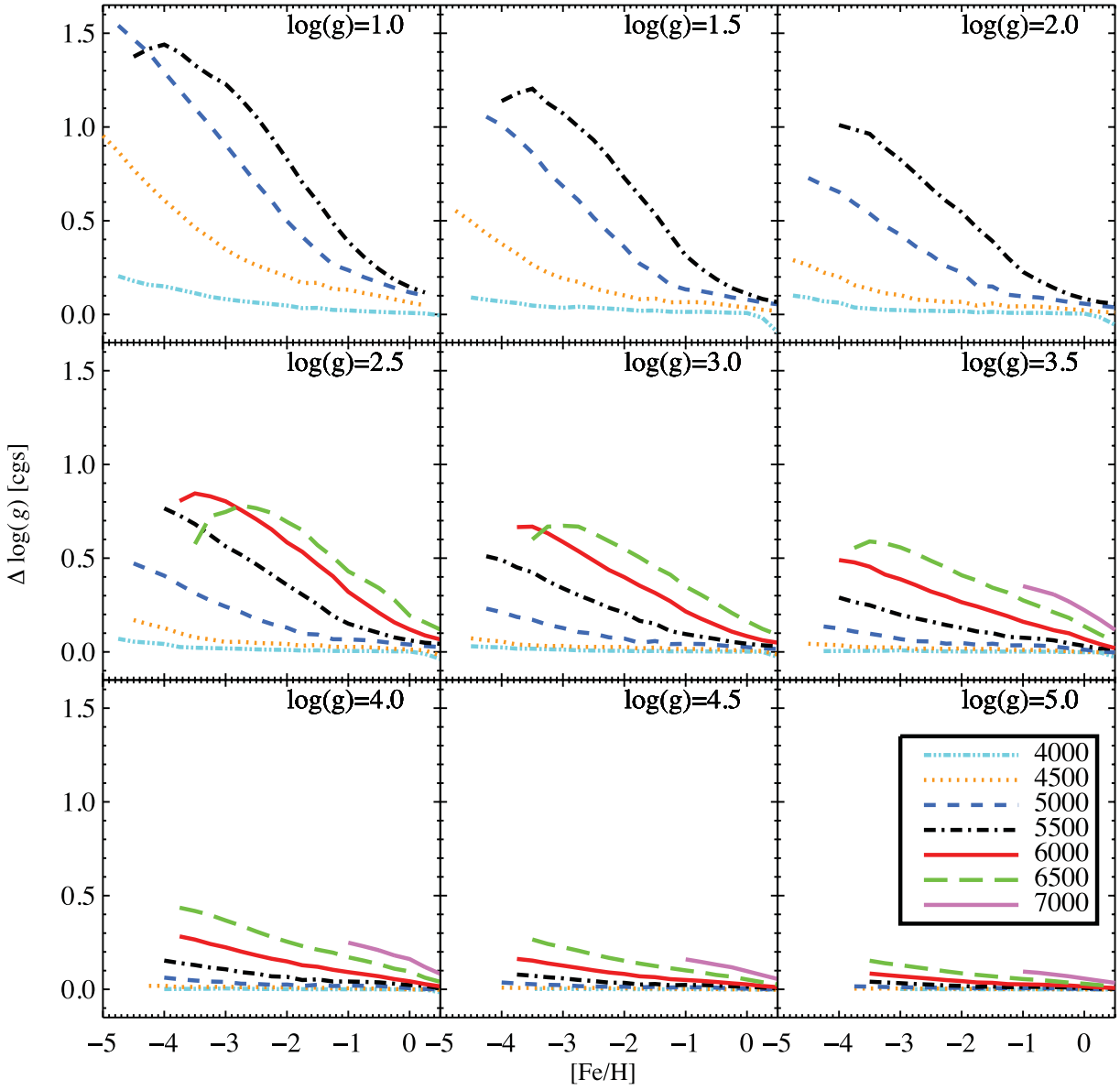

Figure 4. The lines mark the estimated NLTE effect on surface gravities derived from the ionization balance of high-excitation, unsaturated Fe I and Fe II lines, given that other stellar parameters are fixed by independent means. All models shown have $\xi_t = 2.0\,\mathrm{km\,s^{-1}}$.

spectra of late-type stars). The method exploits the larger temperature sensitivity of low-excitation lines compared to high-excitation lines, which simultaneously makes them more sensitive to departures from LTE. For 1D models, NLTE abundance corrections are nevertheless only mildly differential with excitation potential, but they become very significant for metal-poor ⟨3D⟩ models, as illustrated in Paper I.

We have estimated the difference between 1D LTE and NLTE effective temperatures derived through excitation equilibrium, by again interpolating the LTE curves of growth on to NLTE results for all grid points and enforced a flat trend with excitation potential. Again, we restricted ourselves to unsaturated lines, but the only restriction made in excitation potential was that at least one transition must originate from above 3.5 eV. Fig. 6 shows the typical difference in effective temperature derived in the two cases, i.e. $\Delta T_{\mathrm{eff,exc}} = T_{\mathrm{eff,NLTE}} - T_{\mathrm{eff,LTE}}$. Because NLTE abundance corrections are generally more positive for low-excitation lines, the effective temperatures derived through LTE analysis are usually higher. Not surprisingly, the effect tends to increase in tandem with the NLTE effects, but the shape of curves is somewhat different. Down to metallicities as low as [Fe/H] = −3, the curves are rather flat and all types of dwarfs and the bulk of red giant branch stars are affected by less than 50 K. Excitation temperatures derived with 1D models are thus not heavily influenced by NLTE effects except for horizontal branch stars and extremely metal-poor stars. However, we caution that even 1D NLTE results are not reliable in situations where 3D effects are pronounced, in particular if departures from LTE are minor.

3.2.4 Microturbulence

The NLTE abundance corrections show a dependence on line strength beyond saturation ($W_\lambda \gtrsim 50\,\mathrm{m\AA}$), which will impact on the determination of microturbulence from Fe I lines. While the

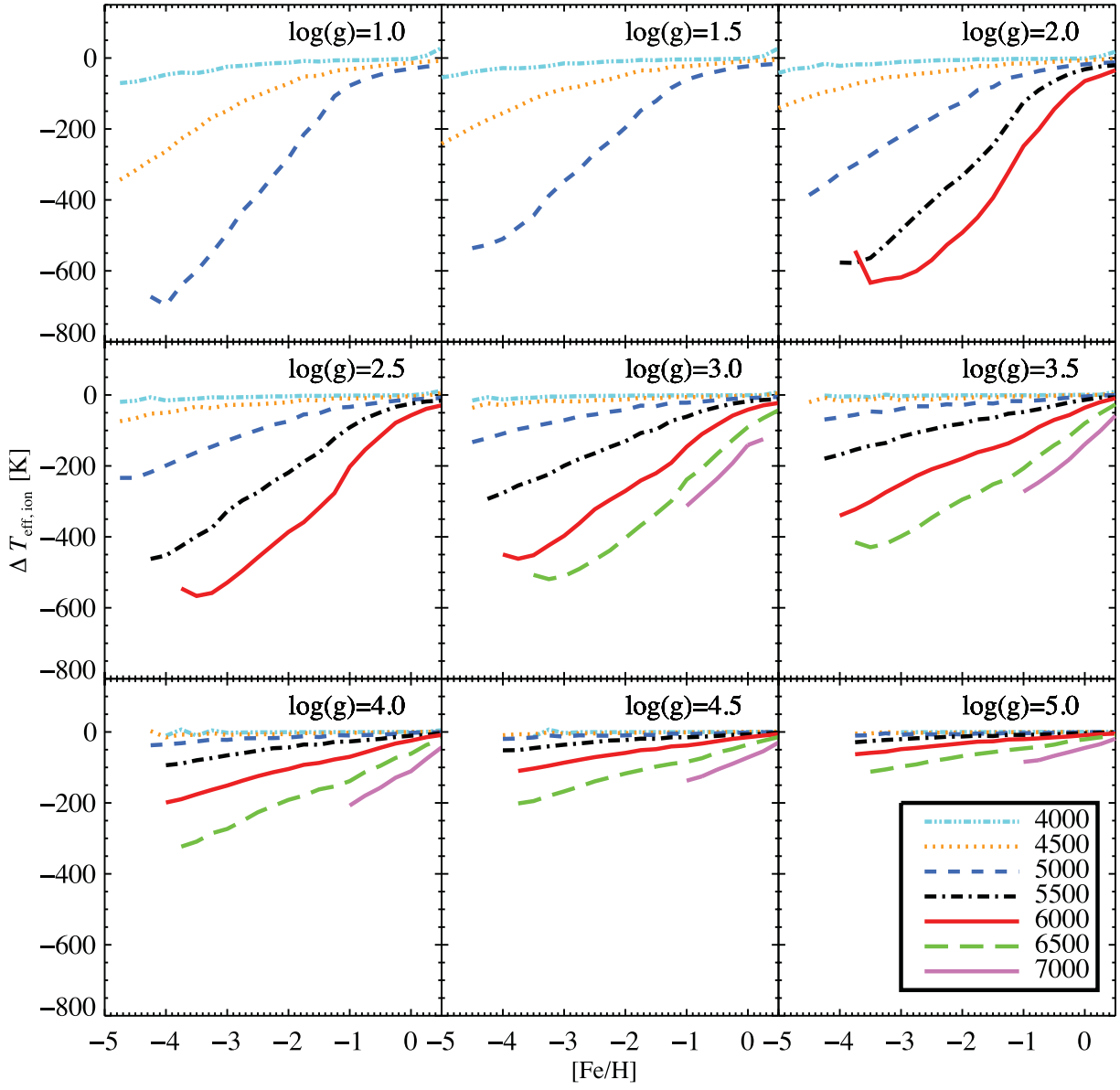

Figure 5. The lines mark the estimated NLTE effect on effective temperatures derived from the ionization balance of high-excitation, unsaturated Fe I and Fe II lines, given that other stellar parameters are fixed by independent means. All models shown have $\xi_t = 2.0\,\mathrm{km\,s^{-1}}$.

effect may be quite significant for individual lines, the typical change is very small. As a general rule, saturated ($50 \lesssim W_\lambda \lesssim 100$ mÅ) lines have an abundance correction that is larger than for unsaturated lines, the difference being roughly a factor of 5 less than the NLTE abundance correction itself in logarithmic units. Ultimately, this leads to lower microturbulent velocities in LTE compared to NLTE.

The size of this effect is illustrated in Fig. 7. These results have been obtained analogously to the other parameters by calculating the microturbulence value that flattens the LTE abundance dependence on reduced equivalent width, using the NLTE equivalent widths as reference in each grid point. The calculations were restricted to high-excitation lines, to minimize a systematic bias as explained above. We also introduced an upper cut in line strength at $\log(W_\lambda/\lambda) = -4.6$ to exclude the damping part of the curve of growth. Similarly to the excitation balance, the effect is essentially negligible for dwarfs and giant stars above [Fe/H] ≥ -3. Extremely metal-poor stars are more affected, but generally they have few lines that are sensitive to this parameter.

3.3 Modelling uncertainties

3.3.1 Model atmospheres

Accurate absolute abundances in LTE and NLTE require realistic model atmospheres, hence spectrum synthesis based on 3D hydrodynamical models is expected to give superior results. Our first attempts to investigate this problem in LTE and NLTE using the averages of the 3D simulations of stellar convection were illustrated in Paper I for selected well-observed stars. We found that the average metallicities derived from ⟨3D⟩ models are not dramatically different from 1D models, in particular in NLTE ($\lesssim$0.04 dex). Most sensitive to the model structure are abundances derived from saturated, low-excitation lines in metal-poor stars. The greater

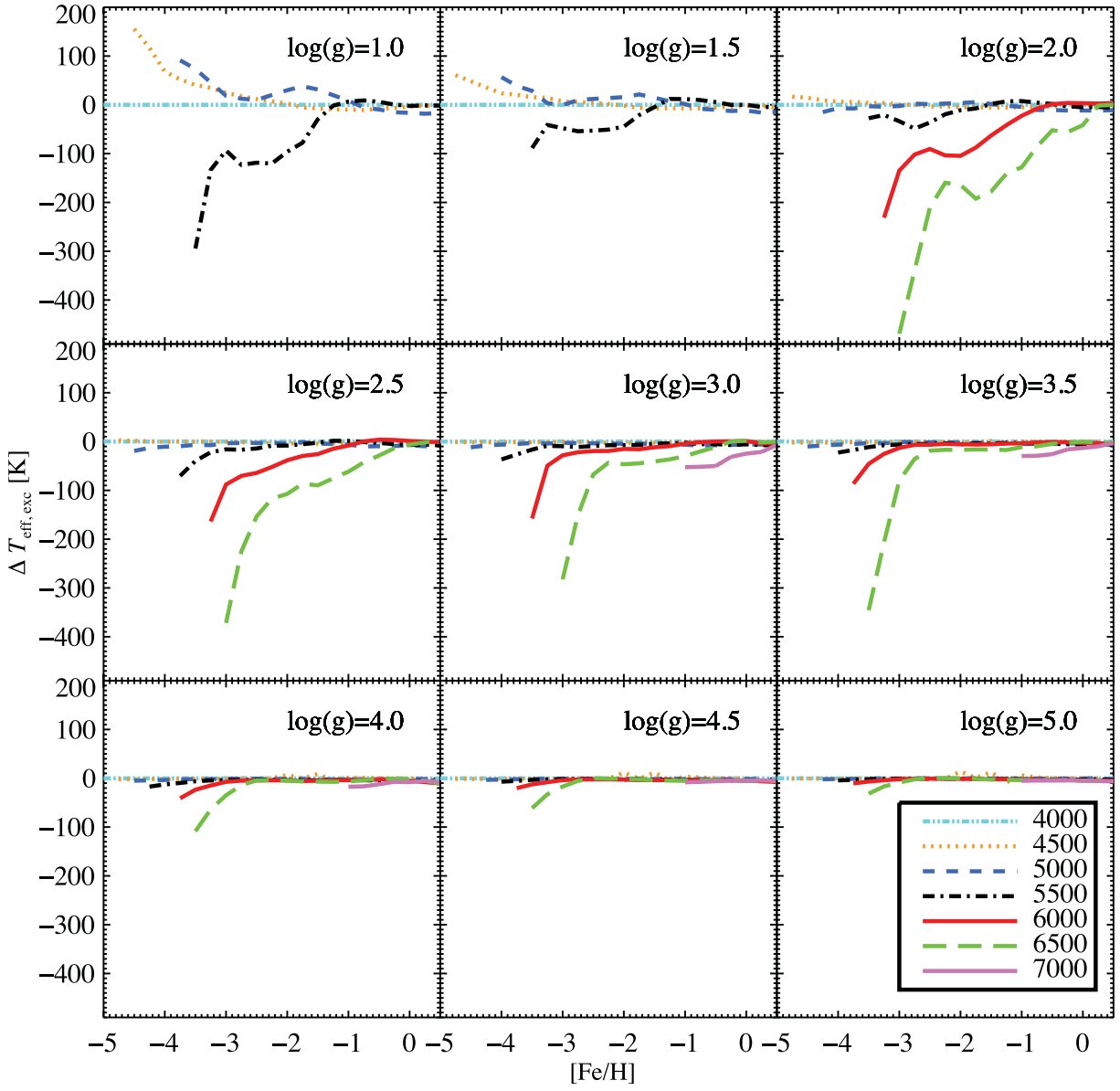

Figure 6. The lines mark the estimated NLTE effect on effective temperatures derived from the excitation balance of unsaturated Fe I lines, given that other stellar parameters are fixed by independent means. All models shown have $\xi_t = 2.0\,\mathrm{km\,s^{-1}}$.

similarity between NLTE abundances of 1D and ⟨3D⟩ models can be understood simply via the close resemblance of the mean radiation field throughout the atmospheres, as it is largely set by conditions at continuum optical depth $\tau_{500\,\mathrm{nm}} \gtrsim 1$, contrary to the Planck function that behaves very differently in shallow atmospheric layers. Paper I also illustrates how stellar parameters inferred through ionization equilibrium of Fe I and Fe II lines agree well with NLTE modelling in 1D and ⟨3D⟩. We emphasize, however, that the excitation equilibrium established with ⟨3D⟩ models is generally superior to that of 1D models. Finally, it is worth to note that the uncovered dependencies of the departures from LTE on the stellar parameters are likely to hold true for any type of model atmosphere grid.

3.3.2 Atomic data

Our analysis focuses on systematic differences between LTE and NLTE, which are not affected by the choice of oscillator strengths and broadening data adopted for spectrum synthesis. According to our assessment, atomic data for level energies, radiative transition probabilities and photoionization cross-sections are sufficiently advanced and complete not to introduce large uncertainties in the modelling. Also, according to our tests the remaining uncertainties in the electron impact collision rates do not introduce large uncertainties in the NLTE modelling. As mentioned in the introduction the most critical parameter is the efficiency of collisions with neutral hydrogen, which we constrained empirically in Paper I. Lowering the scaling factor S_H by one order of magnitude, from 1.0 to 0.1, increases the NLTE effects by typically a factor of 2–4, depending on the stellar parameters. The qualitative behaviour remains the same, but the influence of the radiative-rate imbalance that causes overionization increases. Paper I demonstrates that such large NLTE effects are unrealistic for metal-poor dwarfs and subgiant stars, but are potentially more successful for the metal-poor giant HD122563. Here, we have chosen to

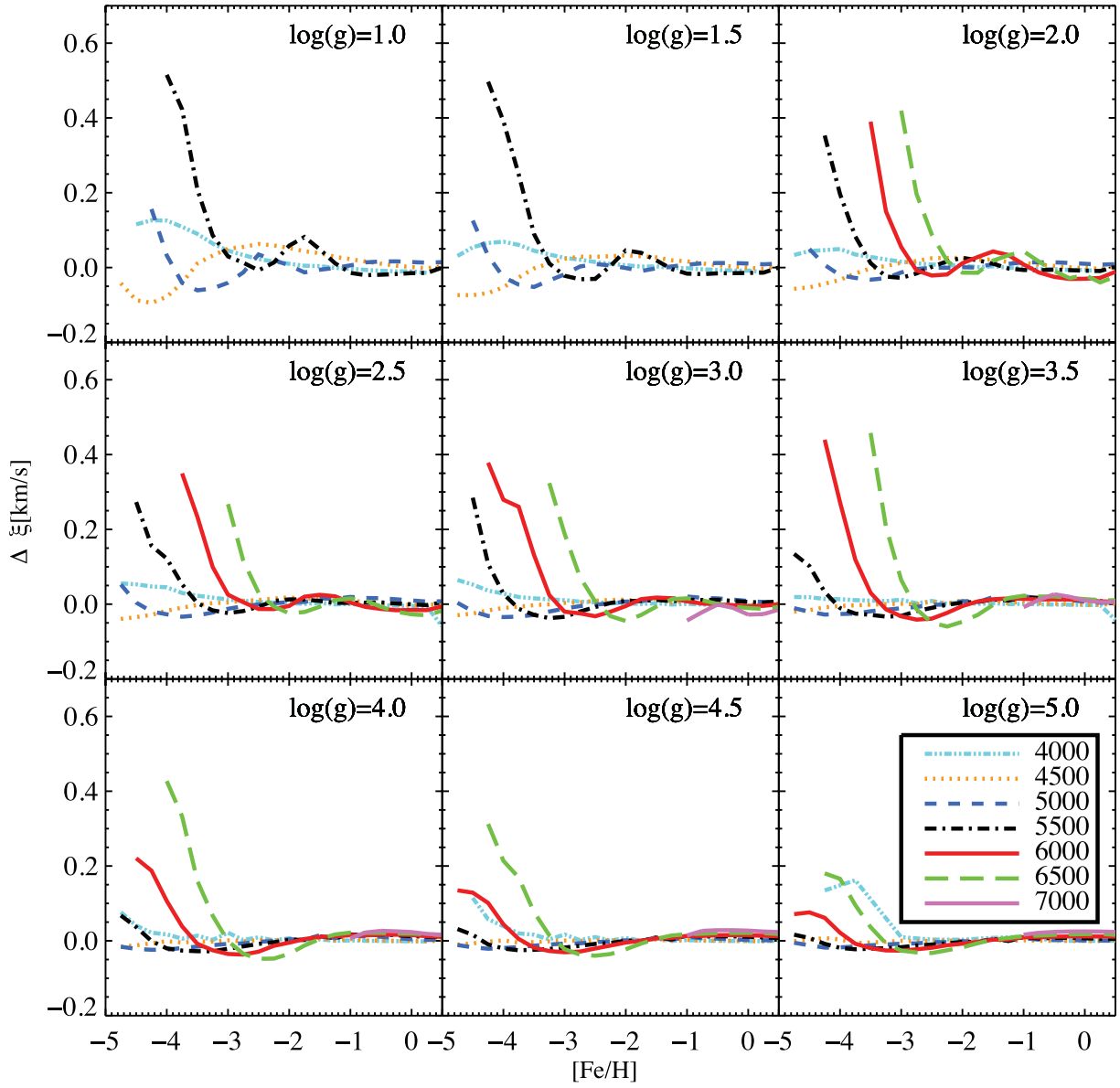

Figure 7. The lines mark the estimated NLTE effect on microturbulent velocities derived from high-excitation Fe I lines, given that other stellar parameters are fixed by independent means. The reference value in LTE is 1 km s^{-1}.

calculate the NLTE grid for $S_{\rm H} = 1.0$, the most supported value, only.

3.3.3 The trace element assumption

As mentioned in the introduction we solve the restricted NLTE problem, which neglects all potential feedback that the perturbed Fe level populations have on the atmospheric structure. This simplification is necessary to make the computations tractable and the consequences have not been rigorously investigated. The most noteworthy implicit assumptions are that the demonstrated changes in the excitation and ionization balance have no significant implications for the free electron density and the UV bound–bound and bound–free opacity. Given the known size of the LTE departures over the late-type star grid, we now proceed to make simple tests of the extent of such a feedback.

The main opacity change would be caused by the lower amount of neutral iron compared to LTE, which in practice can be mimicked with an atmosphere of lower metallicity. Furthermore, NLTE populations of iron would provide more free electrons in the atmosphere. The increase in electron number density can be straightforwardly estimated by the decrease in neutral iron, since each additional iron ion corresponds to one additional electron. It turns out that this effect is negligible over the whole stellar grid, since the free electron density is typically much larger than that of neutral iron (hydrogen and metals with lower ionization potential are the main electron donors). In the most extreme case, the electron density of a cool, metal-rich giant would change by $\lesssim$1 per cent, which is insignificant in this context. We therefore disregard the second aspect and focus our test on the opacity change.

We selected a few models from the grid and performed new NLTE calculations on models with the same stellar parameters, but with a metallicity lower by the mean NLTE correction. The lower

metallicity was also adopted for the calculation of continuous and line background opacity. Thereafter, we compared the LTE and NLTE equivalent widths for a given abundance, obtained from the two different model atmospheres. We performed the test on a metal-rich and metal-poor dwarf and giant with the same parameters as shown in Fig. 3.

The solar metallicity models have a higher sensitivity to the metal content and are more affected by the mentioned inconsistency, even though the predicted sizes of the NLTE corrections are much smaller than for metal-poor stars. In particular, continuous opacities in the UV decrease when the model metallicity is lowered. We thus expect equivalent widths of Fe lines to increase due to lowered continuous opacities, while the NLTE effects are expected to increase and weaken the Fe I lines with respect to LTE. In practice, the NLTE equivalent widths inferred from the model with $T_{\rm eff} = 6500$ K and $\log g = 4.0$ increase by up to 1 per cent when the model metallicity (not the abundance used for computing synthetic line profiles) is lowered by 0.03 dex, corresponding to the mean NLTE abundance correction. This is certainly a second-order effect, approximately 10 times smaller than the NLTE effect itself.

Note that our test implicitly assumes that all the ionization balance of all other elements are similarly affected by NLTE as Fe, which is not the case. Only consistent NLTE model atmosphere calculations will tell for sure how realistic the trace element assumption is for Fe and other elements. Short & Hauschildt (2005) present such a model for the Sun, displaying a dramatic increase in UV flux in NLTE compared to LTE, and a significantly more shallow atmospheric temperature structure at continuum-forming regions. However, their comparison to observed absolute solar fluxes suggests that the opacity loss due to overionization of iron-peak elements is overestimated, or, alternatively, that other important sources of opacity are yet missing.

3.4 Comparison with other studies

Mashonkina et al. (2011) demonstrated in detail how recent developments in atomic data calculations have improved the NLTE modelling of iron lines. In particular, R. L. Kurucz's calculations of high excitation energy levels beyond reach of experiments have enabled a realistic coupling to the next ionization state, without having to enforce an arbitrary thermalization above a certain energy threshold (see also Gehren et al. 2001). As described in Paper I, our NLTE calculations for standard stars are in good quantitative agreement with those of Mashonkina et al. (2011). In Mashonkina (2011), the author presents a small grid of calculations for A–F type dwarfs of solar metallicity. Their NLTE abundance corrections are of similar order of magnitude to ours, but differences for individual Fe I lines can amount to more than 0.05 dex, which is comparable to the size of corrections for solar metallicity stars. There could be many reasons for this; among them are different choices of scaling factor of hydrogen collisions. However, the dependence on surface gravity and effective temperature also show contradictory behaviour, which is surprising. While our NLTE corrections for e.g. Fe I λλ528.179, 521.792 nm increase gradually towards higher effective temperatures, those of Mashonkina rather display a flat behaviour or even decrease. Part of the solution might lie in the adoption of different oscillator strengths, placing the lines on slightly different parts of the curve of growth.

Of earlier studies we highlight Thévenin & Idiart (1999) who derived metallicities in NLTE for a sizeable sample of metal-poor and metal-rich dwarfs and subgiants. They report a strong tendency of increasing NLTE effects with decreasing metallicity, akin to our findings but of greater magnitude. The reason for the difference is likely due to different model atoms; their atom lacked e.g. the important high excitation levels mentioned above.

3.5 Conclusions

The most important NLTE effect for the determination of spectroscopic stellar parameters of late-type stars is the perturbed ionization equilibrium of Fe I and Fe II lines. Departures from NLTE are significant for the derivation of Fe abundances from neutral lines, at the level of $\lesssim$0.1 dex in solar metallicity stars and $\lesssim$0.5 dex in metal-poor stars, while mostly insignificant for Fe II lines. Surface gravities obtained through the ionization balance of neutral and singly ionized lines are consequently affected by 2.5–3 times the typical NLTE abundance correction, in logarithmic units. Cooler stars are less affected than hotter, and dwarfs are less affected than giants, in a well-behaved pattern that can be understood by the variation of radiative and collisional rates over the Hertzsprung–Russell (HR) diagram.

Due to the demonstrated impact of ⟨3D⟩ effects on the Fe line formation (Bergemann et al. 2012), we advice particular caution with temperatures derived through excitation equilibrium of metal-poor stars. 1D LTE effective temperatures are likely to be underestimated in this regime and 1D NLTE effective temperature possibly even more so. However, except for extremely metal-poor stars and high-temperature giants, the NLTE effects on the excitation balance in 1D are typically $\lesssim$50 K. Microturbulence values determined from Fe I lines are likewise very little affected by NLTE for these stars.

Our grid calculations can be used to infer individual NLTE abundances for thousands of lines in late-type stellar spectra. It may be readily predicted that the field of Galactic archaeology subsequently will be confronted with a minor compression of metallicity distribution functions, due to the strictly increasing NLTE effects at lower metallicity. For example, a distribution function of the Galactic halo made up of $T_{\rm eff} = 5000$ K/$\log g = 2.0$ giants would be affected by +0.3 dex at the hyper-metal-poor end, while the metal-rich end would remain essentially unchanged. On the other hand, the relative abundances of dwarf and giant stars may well be little affected, since dwarf samples are commonly hotter than giant samples, and consequently they are prone to departures from LTE of similar sizes. For example, the NLTE corrections of giants of the type just mentioned follow essentially the same behaviour as those of $T_{\rm eff} = 6500$ K/$\log g = 4.0$ dwarfs.

The propagated NLTE effects on Fe I lines on spectroscopic parameters are large enough to affect the classification of evolutionary states, ages and masses. Forced with the requirement to meet the ionization balance of Fe I and Fe II, LTE analysis will underestimate surface gravities and/or overestimate effective temperatures, hence moving stars either upwards or leftwards in the HR diagram. Finally, trends of element ratios, [X/Fe], with respect to [Fe/H] are likely to undergo a change of shape. Assuming no change in element X, negative slopes will become flatter and positive slopes steeper.

In the end, accurate Fe abundances are in general a prerequisite for the accurate determination of abundances of all other elements.

ACKNOWLEDGMENT

We extend our thanks to M. Bautista for assisting with the implementation of the most recent data for photoionization.

REFERENCES

Allen C. W., 1973, Astrophysical Quantities, 3rd edn. Athlone Press, London
Asplund M., 2005, ARA&A, 43, 481
Barklem P. S., Aspelund-Johansson J., 2005, A&A, 435, 373
Barklem P. S., Piskunov N., O'Mara B. J., 2000, A&AS, 142, 467
Bautista M. A., 1997, A&AS, 122, 167
Bergemann M., Lind K., Collet R., Magic Z., Asplund M., 2012, MNRAS, in press (Paper I, doi:10.1111/j.1365-2966.2012.21687.x)
Carlsson M., 1986, Uppsala Astronomical Observatory Reports, 33
Carlsson M., 1992, in Giampapa M. S., Bookbinder J. A., eds, ASP Conf. Ser. Vol. 26, Cool Stars, Stellar Systems, and the Sun. Astron. Soc. Pac., San Francisco, p. 499
Collet R., Asplund M., Thévenin F., 2005, A&A, 442, 643
Collet R., Magic Z., Asplund M., 2011, J. Phys. Conf. Ser., 328, 012003
Cram L. E., Lites B. W., Rutten R. J., 1980, ApJ, 241, 374
Gehren T., Korn A. J., Shi J., 2001, A&A, 380, 645
Grevesse N., Asplund M., Sauval A. J., 2007, Space Sci. Rev., 130, 105
Gustafsson B., Edvardsson B., Eriksson K., Jørgensen U. G., Nordlund Å., Plez B., 2008, A&A, 486, 951
Korn A. J., Shi J., Gehren T., 2003, A&A, 407, 691
Kurucz R. L., 2007, http://www.kurucz.harvard.edu/atoms/2600/gf2600.lines (2008 July 24), http://www.kurucz.harvard.edu/atoms/2601/gf2601.pos (2010 July 23)
Ludwig H., Caffau E., Steffen M., Freytag B., Bonifacio P., Kučinskas A., 2009, Mem. Soc. Astron. Ital., 80, 711
Mashonkina L., 2011, in Romanyuk I. I., Kudryavtsev D. O., eds, Proc. Int. Conf., Magnetic Stars 2010. Special Astrophysical Observatory, Zelenchukskaya, p. 314
Mashonkina L., Gehren T., Shi J.-R., Korn A. J., Grupp F., 2011, A&A, 528, A87
Ralchenko Y., Kramida A. E., Reader J., NIST ASD Team, 2012, NIST Atomic Spectra Database (version 4.1)
Rutten R. J., 2003, in Utrecht University Lecture Notes: Radiative Transfer in Stellar Atmospheres, 8th edn
Seaton M. J., 1962, Proc. Phys. Soc., 79, 1105
Short C. I., Hauschildt P. H., 2005, ApJ, 618, 926
Steenbock W., Holweger H., 1984, A&A, 130, 319
Takeda Y., 1994, PASJ, 46, 53
Thévenin F., Idiart T. P., 1999, ApJ, 521, 753
Unsöld A., 1955, Physik der Sternatmospharen, MIT besonderer Berucksichtigung der Sonne. Springer, Berlin
van Regemorter H., 1962, ApJ, 136, 906

This paper has been typeset from a TEX/LATEX file prepared by the author.